ARTICLE

doi:10.1038/nature11133

Rab5 is necessary for the biogenesis of the endolysosomal system *in vivo*

Anja Zeigerer[1], Jerome Gilleron[1], Roman L. Bogorad[2], Giovanni Marsico[1], Hidenori Nonaka[1], Sarah Seifert[1], Hila Epstein-Barash[3], Satya Kuchimanchi[3], Chang Geng Peng[3], Vera M. Ruda[4], Perla Del Conte-Zerial[1], Jan G. Hengstler[5], Yannis Kalaidzidis[1,6], Victor Koteliansky[2,3] & Marino Zerial[1]

An outstanding question is how cells control the number and size of membrane organelles. The small GTPase Rab5 has been proposed to be a master regulator of endosome biogenesis. Here, to test this hypothesis, we developed a mathematical model of endosome dependency on Rab5 and validated it by titrating down all three Rab5 isoforms in adult mouse liver using state-of-the-art RNA interference technology. Unexpectedly, the endocytic system was resilient to depletion of Rab5 and collapsed only when Rab5 decreased to a critical level. Loss of Rab5 below this threshold caused a marked reduction in the number of early endosomes, late endosomes and lysosomes, associated with a block of low-density lipoprotein endocytosis. Loss of endosomes caused failure to deliver apical proteins to the bile canaliculi, suggesting a requirement for polarized cargo sorting. Our results demonstrate for the first time, to our knowledge, the role of Rab5 as an endosome organizer *in vivo* and reveal the resilience mechanisms of the endocytic system.

What are the molecular mechanisms underlying the biogenesis, number and size of cellular organelles? Organelles of the biosynthetic and endocytic pathway possess a toolbox of coat components, Rab GTPases, SNARE proteins, phosphoinositides and motors that collectively confer functional specificity[1–5]. Whether any of these is a critical component for organelle biogenesis remains an unsolved problem. In the endocytic system, internalized cargo is transported through a network of hundreds of dynamically interacting early endosomes (EEs). These are pleomorphic organelles consisting of a vacuolar part, where cargo to be degraded accumulates, and tubular structures that deliver recycling cargo to the surface[1,6]. Cargo destined for degradation is transferred from EEs to late endosomes via Rab conversion[7,8] or vesicular transport[9]. The number of EEs depends on: (1) *de novo* generation (assuming that clathrin-coated vesicles (CCVs) can fuse homotypically rather than with pre-existing endosomes[6]), (2) homotypic fusion[7,10,11] (reducing the number), (3) homotypic fission that generates new endosomes[7,12], and (4) early-to-late endosome conversion[7] (decreasing the number). Homotypic fusion and fission events are common features of membrane organelles and the main determinants of EE number and size[5,6]. Heterotypic fission that splits tubular structures containing recycling cargo from the vacuolar part can change the size but not the number of EEs. Endosomal trafficking also mediates the delivery of newly synthesized proteins to the plasma membrane[13–15], a function especially important for polarized cargo sorting in epithelial cells[16,17]. Some apical and basolateral proteins are thought to pass through a recycling endosomal intermediate[18–21], but whether EEs are required for biosynthetic transport is unclear. As a central hub of a complex protein network governing membrane tethering, fusion and motility, the small GTPase Rab5 has been proposed to be a master regulator of EEs biogenesis[22]. This concept has received support from studies *in vitro*, where assembly of the Rab5 machinery on proteoliposomes with SNAREs led to efficient membrane fusion[23]. Until now the role of Rab5 in endosome biogenesis *in vivo* has not been addressed as studies in mammalian cells and *Drosophila* have concentrated on endocytosis and synaptic vesicles trafficking[24–26]. Here, to address this outstanding problem, we focused on four main questions. Is Rab5 required for endosome biogenesis? If so, which consequences can decreasing Rab5 have for EEs? The levels of Rab5 may decline proportionally on all endosomes leading to endosome fragmentation[10,27]. Alternatively, the levels of Rab5 per endosome may not change, whereas the total number of endosomes may decrease. Are EEs rate-limiting for late endocytic compartments? To what extent are EEs required for biosynthetic transport in polarized cells? To answer these questions we used a combination of mathematical modelling and *in vivo* short interfering RNA-based technology[28] to efficiently knockdown Rab5 in adult mouse liver.

Results

Modelling of endosome dependency on Rab5

To predict the dependency of the endocytic system on the levels of Rab5, we developed a simple mathematical model. We have previously described a model based on ordinary differential equations describing the Rab5 GDP/GTP cycle, effectors recruitment and Rab5-to-Rab7 conversion[29]. Here, we expanded this model to include the number of endosomes (Methods and Supplementary Information, Box 1). The two components of the Rab5 cycle, shuttling between membrane and cytosol, and GDP/GTP exchange, were represented in a coarse-grained model. Single kinetic steps were grouped as non-linear rate dependencies on active Rab5, which could be monitored through the recruitment of its representative effector, EEA1. To model the number of endosomes, we added the Rab5-dependency of fusion and fission[7,10–12,23]. Note that in this model the ratios of the kinetic rates define the system steady-state behaviour instead of individual parameters. In the model, we considered four main scenarios (Fig. 1, Supplementary Information and Supplementary Fig. 1):

(1) Both homotypic fusion and fission rates are independent of Rab5, implying that other components, for example, SNAREs[30], are rate-limiting. In this (negative control) case, the number of

[1]Max Planck Institute of Molecular Cell Biology and Genetics, 01307 Dresden, Germany. [2]Koch Institute for Integrative Cancer Research, Massachusetts Institute of Technology, Cambridge, Massachusetts 02139, USA. [3]Alnylam Pharmaceuticals, Inc., Cambridge, Massachusetts 02142, USA. [4]Cardiovascular Research Center and Center for Human Genetic Research, Massachusetts General Hospital and Harvard Medical School, Boston, Massachusetts 02114, USA. [5]Leibniz Research Centre for Working Environment and Human Factors (IfADo), 44139 Dortmund, Germany. [6]Belozersky Institute of Physico-Chemical Biology, Moscow State University, 119899, Moscow, Russia.

BOX 1

Model coupling the Rab5 cycle to the endosome number

$$\frac{d\mathrm{Rab5_{ee}}}{dt} = -\mathrm{Rab5_{ee}}\cdot\frac{dN}{dt}\cdot\frac{1}{N} - k_{GAP}(\mathrm{Rab5_{ee}})\cdot\mathrm{Rab5_{ee}} + k_{GEF}(\mathrm{Rab5_{ee}})\cdot\mathrm{rab5_{ee}}$$

$$\frac{d\mathrm{rab5_{ee}}}{dt} = -\mathrm{rab5_{ee}}\cdot\frac{dN}{dt}\cdot\frac{1}{N} - k_{GEF}(\mathrm{Rab5_{ee}})\cdot\mathrm{rab5_{ee}} + k_{GAP}(\mathrm{Rab5_{ee}})\cdot\mathrm{Rab5_{ee}} + k_1\cdot\mathrm{rab5_{cyt}} - k_{-1}\cdot\mathrm{rab5_{ee}}$$

$$\frac{d\mathrm{rab5_{cyt}}}{dt} = -k_1\cdot N\cdot\mathrm{rab5_{cyt}} + k_{-1}\cdot\mathrm{rab5_{ee}}\cdot N$$

$$\frac{dN}{dt} = -k_{fus}(\mathrm{Rab5_{ee}})\cdot N^2 + k_{fis}(\mathrm{Rab5_{ee}})\cdot N$$

Where: $\mathrm{Rab5_{ee}}$, number of active Rab5 per endosome; $\mathrm{rab5_{ee}}$, number of inactive Rab5 per endosome; $\mathrm{rab5_{cyt}}$, total amount of inactive Rab5 in the cytosol; N, number of endosomes; $k_{GEF}(\mathrm{Rab5_{ee}})$ and $k_{GAP}(\mathrm{Rab5_{ee}})$, rates of Rab5 activation and inactivation; $k_{fus}(\mathrm{Rab5_{ee}})$ and $k_{fis}(\mathrm{Rab5_{ee}})$, endosome fusion and fission rates; k_1, recruitment of Rab5 from cytosol; k_{-1}, extraction of Rab5 from early endosomes.

endosomes should not change (Fig. 1a, green line), whereas the amount of EEA1 per endosome would be reduced (Fig. 1b, green).

(2) The fusion but not fission rate depends on Rab5 or (3) the fusion rate depends on Rab5 and the fission rate is a power-law function of the fusion rate. Both lead to endosome fragmentation (Fig. 1a, blue and purple lines), whereas the amount of EEA1/endosome decrease even faster than in scenario 1 (Fig. 1b, blue and purple lines).

(4) Both fusion and fission rates are sigmoidal functions of Rab5. This scenario yields the most unexpected results. First, the number of endosomes demonstrates a non-monotonic dependency on Rab5 (Fig. 1a, red line), that is, the number drops in case of both increase (consistent with ref. 27) and decrease in Rab5. Second, the amount of EEA1/endosome shows a weak dependency on Rab5 over one order of magnitude (Fig. 1b, red line).

We next experimentally tested the predictions from the model. For this, a progressive reduction in Rab5 levels is preferable over gene knockout or loss-of-function mutations[25–27].

Hepatocyte-specific Rab5 knockdown in mouse liver

Most of the mechanistic understanding of Rab5 originated from cell-free systems[10,11,23] and cultured cells[7,27]. Rab5 has three isoforms, Rab5a,b,c[24], whose efficient depletion by RNAi in cultured cells causes cell cycle defects[31], making results difficult to interpret. Therefore, we tested the role of Rab5 in endosome biogenesis *in vivo* in an organ where cells are mainly post-mitotic and within their physiological environment. To this end, we took advantage of a novel technology based on lipid nanoparticles (LNPs) for specific delivery of siRNAs to mouse hepatocytes *in vivo*[32,33]. Allowing the packaging of various siRNAs to achieve simultaneous silencing of multiple genes[32,33], this technology is ideal for knocking down all three Rab5 isoforms. Furthermore, the liver provides the opportunity to investigate the role of EEs in cell polarity *in vivo*. Specific Rab5a,b,c siRNAs were selected (Methods and Supplementary Fig. 2a), validated by 5′-RACE *in vivo* (Supplementary Fig. 2b) and incorporated as an equiponderant mixture (Rab5all) into LNPs optimized for liver-specific delivery[32,33]. Control formulations consisted of the same concentration of Luciferase-targeting siRNAs. LNPs were delivered systemically via tail vein injection and displayed an *in vivo* dose response with maximal Rab5 messenger RNA silencing of approximately 80–90% for Rab5a, b, c at 0.5 mg kg^{-1} each (Supplementary Fig. 2c). Rab5 knockdown (Rab5KD) was isoform- (Supplementary Fig. 2d) and liver-specific (Supplementary Fig. 2e). Maximal mRNA silencing of all Rab5 isoforms was achieved after 3 days and lasted at least 5 days, followed by a slow recovery (Fig. 2a). Importantly, LNPs did not produce any detectable inflammatory response or liver toxicity (Supplementary Fig. 3).

The reduction of Rab5 protein was determined by western blot analysis at 3–15 days post-injection using an anti-Rab5 pan antibody (Fig. 2b) recognizing all Rab5 isoforms equally (Supplementary Fig. 2f). We estimated the strongest reduction (~85%) 5 days post-injection (Fig. 2c). Because gene downregulation is mainly restricted to hepatocytes[28], the remaining levels of Rab5 could be accounted by non-parenchymal cells. Interestingly, at 10 days the levels of Rab5 protein partially recovered to approximately 35% of control.

Loss of EEA1 vesicles upon Rab5KD in liver

To determine the impact of Rab5 depletion on intracellular compartments in liver *in vivo*, it was necessary to optimize and further develop *ad hoc* staining protocols for each organelle marker in liver sections.

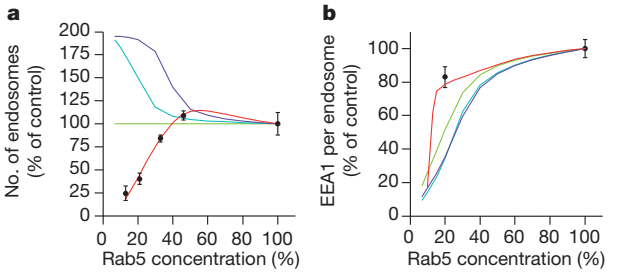

Figure 1 | Mathematical model of endosome number as function of Rab5 levels. **a**, **b**, Model predictions of number of endosomes (**a**) and amount of Rab5 effectors (for example, EEA1) per endosome as function of Rab5 levels for the four scenarios (**b**) (see text). Green line, scenario 1; blue line, scenario 2; purple line, scenario 3; red line, scenario 4. Black dots, experimental results (mean ± s.e.m.).

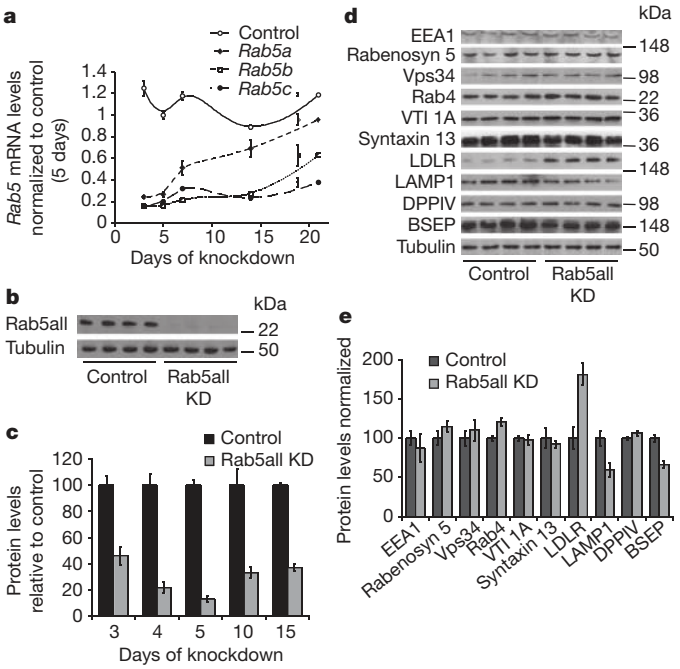

Figure 2 | Time course of *Rab5* mRNA depletion and analysis of protein expression in mouse liver *in vivo*. **a**, Analysis of *Rab5* mRNA levels over 21 days upon Rab5KD in mouse liver *in vivo* (mean ± s.e.m., $n = 3$). **b**, Representative example of western blot analysis of Rab5 protein 5 days post injection ($n = 4$). **c**, Time course of Rab5 protein levels at the indicated times post injection by quantitative western blotting (mean ± s.e.m.). **d**, Western blot analysis of endosomal machinery and cargo from liver lysates 5 days post-injection ($n = 4$). **e**, Quantification of western blots shown in **d** (mean ± s.e.m.).

We first examined the staining pattern of the Rab5 effector and marker of EEs, EEA1 (ref. 34), 5 days after tail vein injection of LNPs. Using quantitative multi-parametric image analysis (QMPIA[35]), we measured a 70% reduction in number of EEA1-positive structures and total intensity of EEA1 on endosomes after Rab5 depletion compared to control (Fig. 3a, b). However, the mean intensity of EEA1/endosome was reduced by only 15%. The loss of EEA1-positive endosomes was not due to a reduction in EEA1 expression, as determined by protein analysis (Fig. 2d, e). Interestingly, knockdown of individual Rab5 isoforms had no effect on EEA1-positive endosomes (Supplementary Fig. 4), indicating that they are (partially) redundant, without excluding specific effects on cargo transport[36]. These results are only consistent with scenario 4 predicting loss of EEs (Fig. 1a) but just a moderate decrease in EEA1 content per endosome (Fig. 1b).

Rab5KD causes loss of EEs, late endosomes and lysosomes

To verify that EE number is indeed reduced, we analysed liver sections by electron microscopy to compare the number of endosomes with the levels of Rab5 protein at each time point. In control sections, EE (large black arrow), late endosome/multi-vesicular bodies (MVBs; thin black arrow) and lysosomes (white arrow) could be discerned on the basis of their characteristic morphology[37,38] (Fig. 4a). Three days post-injection, when the levels of Rab5 were already reduced by approximately 50%, the number of EEs was not significantly altered compared with control. In contrast, at days 4 and 5 when Rab5 was reduced to approximately 15% of total, the results were striking. First, there was a marked reduction in EEs (Fig. 4b), consistent with the decrease in EEA1-positive structures observed by light microscopy (Fig. 3). Interestingly, the mean size of remaining EEs after 4 (246.3 nm ± 9.6, P value = 0.2316) and 5 days (224.8 nm ± 21.5, P value = 0.1247) was only mildly reduced compared to control (289.2 nm ± 37.9). Second, we observed an approximately 80% reduction also in late endosomes/MVBs and lysosomes (Fig. 4c), reflecting the loss of the entire endolysosomal system. Interestingly, at 5 days there was a significant increase in clathrin-coated pits (CCPs) and clathrin-coated vesicles (CCVs) (Fig. 4d), and the basolateral plasma membrane was highly convoluted (Fig. 4b, middle inset), suggesting that endocytosis was inhibited (see below).

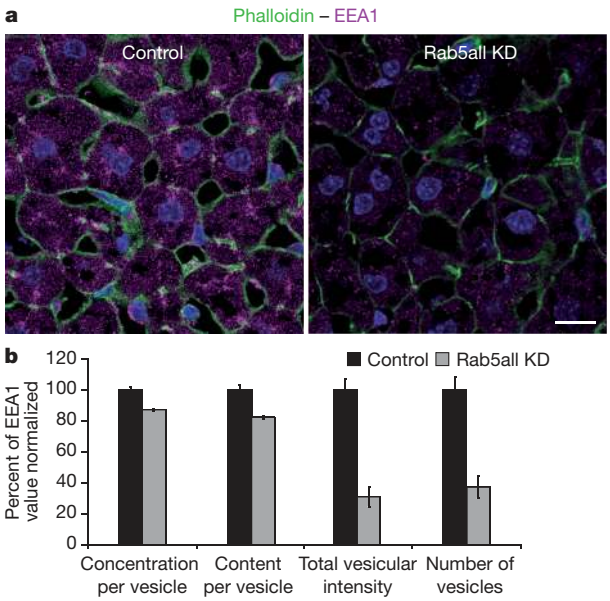

Figure 3 | Loss of EEA1 structures upon Rab5KD *in vivo*. **a**, Representative confocal microscopy images of liver sections stained with anti-EEA1 antibody, phalloidin and DAPI from control and Rab5KD animals (three merged middle confocal sections as maximal projections, see Methods in Supplementary Information). Scale bar, 20 μm. **b**, QMPIA of EEA1 vesicles from four different animals per condition (mean ± s.e.m.).

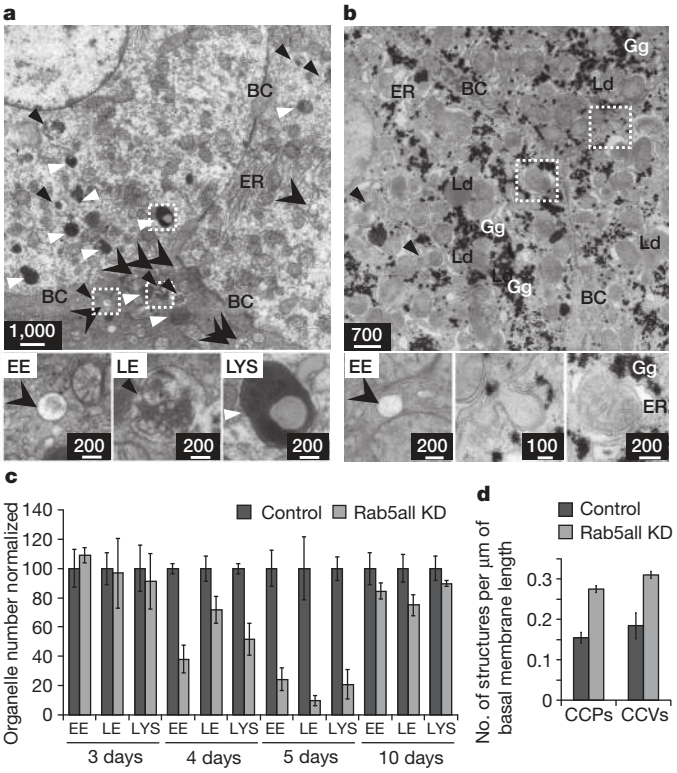

Figure 4 | Loss of early endosomes, MVBs and lysosomes upon Rab5KD. **a**, **b**, Electron microscopy images of control (**a**) and KD (**b**) liver samples 5 days post-injection. BC, bile canaliculi; EE, early endosomes (large black arrow); LE, late endosomes (thin black arrow); LYS, lysosomes (white arrow); ER, endoplasmic reticulum; Gg, glycogen granules; Ld, lipid droplets. Insets show high magnification of representative structures. Convolution of the plasma membrane in Rab5KD (middle inset). Scale bars in nm. **c**, Time-course quantitative analysis of EE, LE and LYS profiles (mean ± s.e.m.). **d**, Quantification of CCPs and CCVs normalized per μm of basolateral membrane 5 days post-injection (mean ± s.e.m.).

Importantly, the phenotype was reversible. After 10 days, when Rab5 recovered to approximately 35% of control (Fig. 2c), the entire endocytic pathway was almost completely rebuilt (Fig. 4c). Notably, these data are entirely consistent with scenario 4 of the mathematical model, predicting changes in endosome number but not in amount of endosomal machinery (EEA1) per endosome (Fig. 3), in response to loss of Rab5 (Fig. 1a, b, black dots). In contrast to endosomes, the organelles of the biosynthetic pathway were much less affected upon Rab5KD. The relative serum levels of albumin and Factor-VII were normal (Supplementary Fig. 3d, e), indicative of functional secretion. We observed swelling of the endoplasmic reticulum (Fig. 4b, right inset), possibly reflecting metabolic perturbations[39]. Indeed, hepatocytes contained numerous lipid droplets and glycogen granules, implying a severe metabolic dysfunction (Fig. 4b, right inset). No alterations of the Golgi complex were detectable by Giantin staining (Supplementary Fig. 5a, b). The number and total intensity of Rab11-positive structures, and the amount of Rab11/structure were only moderately reduced (15%) (Supplementary Fig. 5c, d) demonstrating that recycling endosomes do not disassemble despite loss of EEs. To explore the cause of depletion of endosomal compartments, we inspected established regulators of endosome trafficking (Fig. 2d, e). We did not observe changes in EEA1, Rabenosyn-5, Vps34 and Rab4 in lysates of Rab5KD liver. The levels of the endosomal SNAREs Syntaxin-13 and VTI-1A were unaltered (Fig. 2d, e), indicating that the loss of endosomes is not consequent to the loss of expression of membrane tethering and fusion proteins[23]. However, we detected a 50% decrease in LAMP1, consistent with a loss of late endocytic compartments (Fig. 2d, e and see below). Taken together, these data support the hypothesis that loss of endosomal

compartments is due to failure to assemble the transport machinery on membranes in the absence of Rab5.

Block of low-density lipoprotein uptake upon Rab5KD *in vitro*

The strong perturbations in EEs, late endosomes and lysosomes and the accumulation of CCPs and CCVs detected by EM upon Rab5 depletion prompted us to inspect the effects on endocytosis (Fig. 4d). Interestingly, we observed a strong increase in low-density lipoprotein (LDL) ($0.7015\ mg\ ml^{-1} \pm 0.211$, P value < 0.0001) in the serum of Rab5KD compared to control ($0.0700\ mg\ ml^{-1} \pm 0.039$) animals, arguing for reduced LDL uptake by the liver. To test this hypothesis directly, we measured LDL internalization kinetics. Given the difficulty of performing time-course uptake experiments *in vivo*, we used isolated primary mouse hepatocytes. Five days post-transfection with anti-Rab5all, we observed an approximately 80% reduction in mRNA levels of all Rab5 isoforms (Supplementary Fig. 2g). The number of EEA1-positive endosomes were reduced by about 70%, whereas the amount of EEA1/endosome was decreased only by about 15% (Supplementary Fig. 6a, c), corroborating the *in vivo* results (Fig. 3). LAMP1-positive structures (Supplementary Fig. 6b) and total vesicular intensity were also strongly reduced (~60–70%), again indicating loss of late endosomes/lysosomes (Supplementary Fig. 6d).

Next, we measured endocytosis of fluorescent LDL in primary mouse hepatocytes (Fig. 5). Five days post-transfection QMPIA revealed a marked slow-down in the kinetics of LDL uptake accompanied by a strong (70%) decrease in LDL-positive structures (Fig. 5a–c). These data therefore explain the high levels of LDL in the serum upon Rab5KD. Importantly, there was no downregulation of LDLR on the cell surface (Supplementary Fig. 6e). The total levels of LDLR were even increased *in vivo* (Fig. 2d, e), suggesting a possible compensatory mechanism to overcome the reduction in LDL uptake. To demonstrate that the phenotypic alterations in endosome number are specific for Rab5 depletion, we downregulated (90%) dynamin 2, a multidomain GTPase necessary for vesicle scission from the plasma membrane[40,41] in primary mouse hepatocytes (Supplementary Fig. 7a,b). We observed an almost complete reduction in total LDL uptake and number of LDL vesicles (Fig. 5d, e) but, interestingly, no significant changes in number and intensity of EEA1- and LAMP1-positive structures (Fig. 5f).

Alterations in hepatocyte polarity *in vivo*

The ablation of EEs upon Rab5KD provided the opportunity to examine the dependence of polarized sorting on this endosomal compartment. We first inspected the polarity of hepatocytes by staining liver sections for the tight junction marker ZO1 (Supplementary Fig. 8, middle panels) and actin/phalloidin to detect cell borders and the bile canaliculi network (Supplementary Fig. 8, left panels). The latter was unchanged (Supplementary Fig. 8, right panels), ruling out disruption of cell polarity. We next inspected the localization of three apical proteins, dipeptidylpeptidase 4 (DPPIV), multidrug resistant-associated protein (MRP2) and the major bile salt export pump (BSEP), whose dependence on endosomal transport has never been demonstrated *in vivo*[42]. DPPIV was shown to follow the transcytotic route[43], whereas MRP2 trafficking remains controversial, being transcytosed[43] or following the direct apical targeting pathway[44]. BSEP was suggested to pass through recycling endosomes[42], although direct functional evidence for endosomal intermediates is lacking. In control liver, DPPIV was enriched in the bile canaliculi network where it colocalized with MRP2 (Fig. 6a, upper middle and right panel), with a small fraction on the basal side (Fig. 6a, upper left panel). Strikingly, in Rab5KD liver DPPIV redistributed to the basolateral surface of hepatocytes (Fig. 6a, lower left panel), colocalizing with CD166 and FcyR (Fig. 6b). DPPIV did not accumulate in Rab11-positive recycling endosomes or in the Golgi complex (Fig. 6b), and its expression was unaltered (Fig. 2d, e), indicating that after leaving the biosynthetic pathway DPPIV is trafficked to the basolateral side but fails to be re-internalized and sorted apically. In contrast, MRP2 correctly

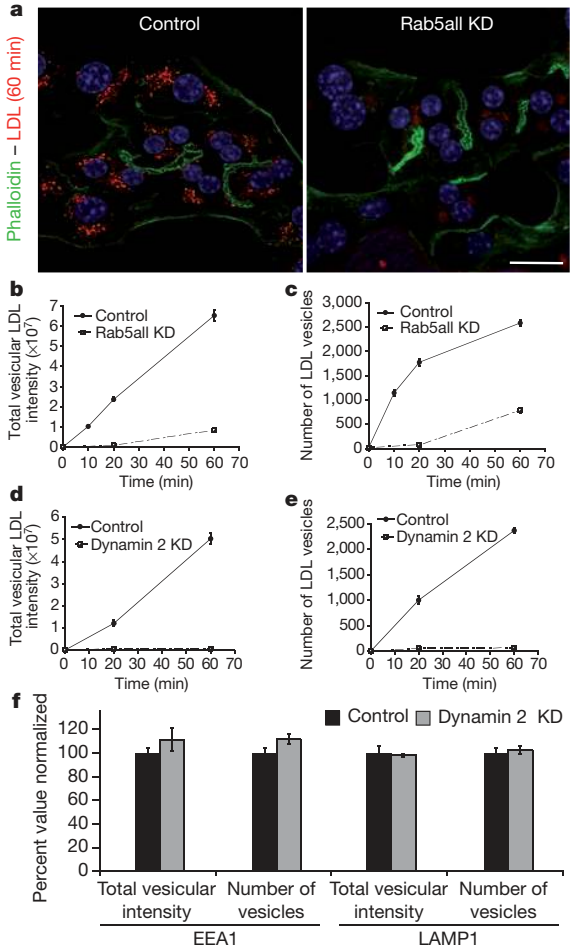

Figure 5 | Block of LDL endocytosis upon Rab5KD in primary hepatocytes *in vitro*. **a**, Representative confocal microscopy images of primary hepatocytes 5 days post-transfection, allowed to internalize DiI (1,1′-dioctadecyl-3,3,3′3′-tetramethylindocarbocyanine perchlorate)-LDL for various time points and stained with Alexa 488-phalloidin and DAPI. Scale bar, 20 μm. **b**, **c**, Time-course internalization of LDL analysed by QMPIA (key parameters are presented) (mean ± s.e.m.). **d**–**f**, Downregulation of dynamin 2 in isolated primary mouse hepatocytes. **d**, **e**, LDL time-course data analysed by QMPIA (mean ± s.e.m.). **f**, Confocal images of primary hepatocytes stained with anti-EEA1 and anti-LAMP1 antibodies and analysed by QMPIA (mean ± s.e.m.).

localized to the apical surface (Fig. 6a, lower middle and right panel), suggesting that it follows a direct route. However, BSEP was greatly reduced (~70%) at the bile canaliculi (Fig. 6c, d) and redistributed intracellularly upon Rab5 depletion (Fig. 6c, inset right panel), indicating that it needs an endosomal intermediate for apical targeting. This strong decrease was not due to a similar reduction in protein expression, because BSEP protein levels were reduced only by approximately 30% (Fig. 2d, e). These results show that ablation of the endolysosomal system caused a strong impairment of transport of selected membrane proteins to the apical surface in hepatocytes *in vivo*. Altogether, our data highlight the functional role of the endocytic system in biosynthetic transport and cell polarity beyond what has been demonstrated so far.

Discussion

The most striking result of this study is that depletion of Rab5 *in vivo* led to loss of approximately 80% of the endolysosomal pathway, showing for the first time that Rab5 is a principal component of EE biogenesis *in vivo*. Other components, such as Rab5 effectors and SNAREs, continue to be expressed but, evidently, are not sufficient for providing structural and functional identity to EEs. Therefore,

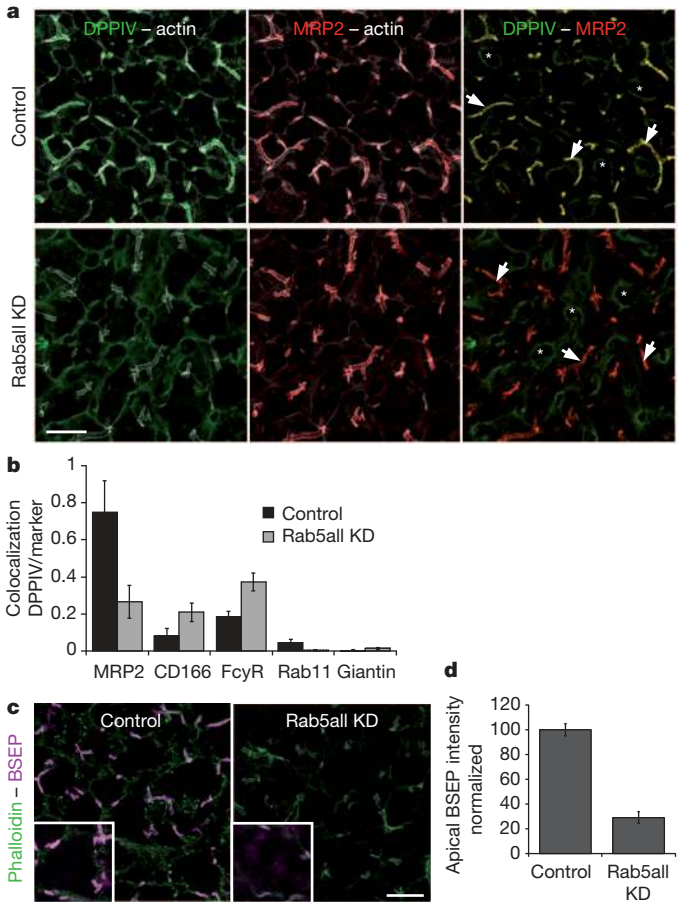

Figure 6 | Rab5KD causes mis-sorting of apical proteins in hepatocytes *in vivo*. **a**, Liver sections from control and Rab5KD animals were stained for DPPIV (left panels), MRP2 (middle panels) and actin. Merged images of DPPIV and MRP2 are shown in the right panels. Arrow, bile canaliculi; asterisk, sinusoids. Scale bar, 20 μm. **b**, QMPIA of DPPIV distribution and colocalization with various markers ($n = 4$) (mean ± s.e.m.). **c**, Images of liver sections stained for BSEP and actin. Scale bar, 20 μm. Insets, high magnification of hepatocytes to visualize BSEP intracellular and apical localization in knockdown samples. **d**, Quantification of apical BSEP fluorescence intensity in control and Rab5KD liver (mean ± s.e.m.).

Rab5 is mandatory for the assembly of the endosomal machinery and not a secondary regulator[45].

An important and unexpected finding is the resilience (defined, in the context of engineering and computing systems, as the ability to withstand and/or recover from strong perturbations) of the endocytic system to wide fluctuations in Rab5 concentrations. Loss of endosomes was not proportional to the levels of Rab5 but occurred abruptly upon around 80% reduction in protein levels (Fig. 2c), supporting only scenario 4 of the mathematical model (Fig. 1a, b). In this scenario, the fusion/fission dependency on Rab5 is a sigmoidal function, implying that wide variations in Rab5 levels result only in minor changes in Rab5 effectors per endosome. By analogy with engineering systems, Rab5 plays the role of the stabilizing element, that is, an element for which small changes are amplified and the feedback loops in the system (GDP/GTP exchange[29] and fusion/fission, Supplementary Fig. 1d, e) suppress variations. Consistent with the model, the finding that EEs were reduced in number, but not size, and retained a constant amount of effectors (Figs 1a, b and 3) suggests that each endosome requires a full complement of Rab5 machinery to be functional. The prediction of moderate decrease in endosome number upon increase in Rab5 is consistent with reported phenotypes[27]. Interestingly, after 10 days Rab5 recovered to approximately 35% of control and the entire endocytic pathway was rebuilt. These data are remarkably consistent with the model predicting even a moderate increase in endosome number with Rab5 reduced to 50% (Fig. 1a). For the interpretation of the phenotype it is important to consider EEs as a network in time rather than individual entities. Endosomes interact with one another within seconds[7]. As Rab5 gradually (over days) decreases upon RNAi, the endosomal network has time to adjust to a new steady state, with fewer endosomes being able to maintain normal amounts of Rab5 machinery. Consequently, EE biogenesis is suppressed and the EE network progressively shrinks. Because decrease in Rab5 reduces the rate of homotypic EE fusion[7,10,11], EEs would be expected to fragment. Yet, we found no evidence of fragmentation. Indeed, our model (Fig. 1) predicted that homotypic EE fission must be affected (possibly indirectly) even more than fusion below threshold (Supplementary Fig. 1b, c). This interpretation is supported by QMPIA of EE populations in LDL pulse-chase studies (Supplementary Information and Supplementary Fig. 9). As fewer EEs can reach the amount of Rab5 necessary for conversion[7,29], the number of late endocytic structures is reduced. This effect is therefore secondary to the loss of EEs. Note that the residual endosomes in the network are still functional, capable of receiving and propagating cargo for degradation (Supplementary Information and Supplementary Fig. 9b). Upon Rab5KD, there may be effects on the heterotypic fission of recycling tubules and vesicles as well. However, Rab11 compartments were reduced in number only by 15% (Supplementary Fig. 5c, d). This mild effect and the surface levels of LDLR being also unchanged (Supplementary Fig. 6e) suggest that recycling may not be dysfunctional (see Supplementary Information).

Given the time scale of the effect (5 days), the 'disappearance' of lysosomes is surprising, because indigestible substances accumulate within lysosomes for weeks[46]. However, lysosomes within hepatocytes are able to release their content into the bile canaliculi by exocytosis[46] and, therefore, such organelles may not have been replaced.

An unresolved problem is whether vesicles derived from the plasma membrane contribute to the biogenesis of EEs[6]. Blockage of dynamin 2-dependent endocytosis did not alter the number of endosomes (Fig. 5f), which is inconsistent with an obligatory role of endocytic vesicles in EEs biogenesis. However, caution in the interpretation is suggested by the possible induction of dynamin-independent compensatory endocytic mechanisms (clathrin-independent carriers (CLICs)/GPI-enriched endocytic compartments (GEECs), Arf6-dependent) that may maintain EEs[47]. Their onset may require time, unlike the use of temperature-sensitive mutants[48].

Liver function depends on the polarity of hepatocytes. Upon loss of Rab5 the delivery of DPPIV and BSEP to the bile canaliculi was strongly impaired (Fig. 6). In contrast, the localization of MRP2, which was postulated to follow a transcytotic route[43] to the bile canaliculi, was unaffected, supporting direct targeting for this transporter[44]. Subcellular fractionation studies indicated that apical proteins traverse endosomal compartments, primarily Rab11-positive recycling endosomes, on their way to the bile canaliculi[42,49]. Our data, however, suggest that EEs are also required as sorting and transport intermediates for the delivery of certain proteins to the apical surface in hepatocytes. Overall, the primary cells and organ system used in this study highlight the importance of using a physiological system to investigate cell polarity and tissue morphogenesis.

METHODS SUMMARY

The following methods are described in detail in Supplementary Information. Modelling was done by simulation and fitting ordinary differential equations (ODEs) using FitModel. LNP siRNA formulations[32,33] were administered to C57BL/6N mice through tail vein injection. Livers were collected after various time points and analysed for mRNA (quantitative PCR with reverse transcription) and protein determination (western blotting), and sectioned for immunocytochemistry and electron microscopy. Western blots were quantified with ImageJ (http://lukemiller.org/index.php/2010/11/analyzing-gels-and-western-blots-with-image-j/). Immunocytochemistry was performed on optimal cutting temperature compound (OCT)-embedded liver cryosections. For electron

microscopy, liver tissues were fixed, embedded and sectioned following classical procedures. Primary mouse hepatocytes were isolated, cultured and subjected to immunofluorescence analysis. LDL internalization assays were performed as described[7]. QMPIA was performed as described[35].

Received 13 December 2011; accepted 3 April 2012.

1. Mellman, I. Endocytosis and molecular sorting. *Annu. Rev. Cell Dev. Biol.* **12,** 575–625 (1996).
2. Bonifacino, J. S. & Glick, B. S. The mechanisms of vesicle budding and fusion. *Cell* **116,** 153–166 (2004).
3. Robinson, M. S. Adaptable adaptors for coated vesicles. *Trends Cell Biol.* **14,** 167–174 (2004).
4. Jahn, R. & Scheller, R. H. SNAREs–engines for membrane fusion. *Nature Rev. Mol. Cell Biol.* **7,** 631–643 (2006).
5. Pfeffer, S. R. Unsolved mysteries in membrane traffic. *Annu. Rev. Biochem.* **76,** 629–645 (2007).
6. Gruenberg, J. & Maxfield, F. R. Membrane transport in the endocytic pathway. *Curr. Opin. Cell Biol.* **7,** 552–563 (1995).
7. Rink, J., Ghigo, E., Kalaidzidis, Y. & Zerial, M. Rab conversion as a mechanism of progression from early to late endosomes. *Cell* **122,** 735–749 (2005).
8. Poteryaev, D., Datta, S., Ackema, K., Zerial, M. & Spang, A. Identification of the switch in early-to-late endosome transition. *Cell* **141,** 497–508 (2010).
9. Vonderheit, A. & Helenius, A. Rab7 associates with early endosomes to mediate sorting and transport of Semliki forest virus to late endosomes. *PLoS Biol.* **3,** e233 (2005).
10. Gorvel, J. P., Chavrier, P., Zerial, M. & Gruenberg, J. rab5 controls early endosome fusion *in vitro*. *Cell* **64,** 915–925 (1991).
11. Rybin, V. *et al.* GTPase activity of Rab5 acts as a timer for endocytic membrane fusion. *Nature* **383,** 266–269 (1996).
12. Skjeldal, F. M. *et al.* The fusion of early endosomes induces molecular motor-driven tubule formation and fission. *J. Cell Science* http://dx.doi.org/10.1242/jcs.092569 (22 February 2012).
13. Futter, C. E., Connolly, C. N., Cutler, D. F. & Hopkins, C. R. Newly synthesized transferrin receptors can be detected in the endosome before they appear on the cell surface. *J. Biol. Chem.* **270,** 10999–11003 (1995).
14. Harsay, E. & Schekman, R. A subset of yeast vacuolar protein sorting mutants is blocked in one branch of the exocytic pathway. *J. Cell Biol.* **156,** 271–286 (2002).
15. Ang, A. L. *et al.* Recycling endosomes can serve as intermediates during transport from the Golgi to the plasma membrane of MDCK cells. *J. Cell Biol.* **167,** 531–543 (2004).
16. Weisz, O. A. & Rodriguez-Boulan, E. Apical trafficking in epithelial cells: signals, clusters and motors. *J. Cell Sci.* **122,** 4253–4266 (2009).
17. Golachowska, M. R., Hoekstra, D. & van IJzendoorn, S. C. D. Recycling endosomes in apical plasma membrane domain formation and epithelial cell polarity. *Trends Cell Biol.* **20,** 618–626 (2010).
18. Ihrke, G. *et al.* Apical plasma membrane proteins and endolyn-78 travel through a subapical compartment in polarized WIF-B hepatocytes. *J. Cell Biol.* **141,** 115–133 (1998).
19. Cresawn, K. O. *et al.* Differential involvement of endocytic compartments in the biosynthetic traffic of apical proteins. *EMBO J.* **26,** 3737–3748 (2007).
20. Nokes, R. L., Fields, I. C., Collins, R. N. & Folsch, H. Rab13 regulates membrane trafficking between TGN and recycling endosomes in polarized epithelial cells. *J. Cell Biol.* **182,** 845–853 (2008).
21. Farr, G. A., Hull, M., Mellman, I. & Caplan, M. J. Membrane proteins follow multiple pathways to the basolateral cell surface in polarized epithelial cells. *J. Cell Biol.* **186,** 269–282 (2009).
22. Zerial, M. & McBride, H. Rab proteins as membrane organizers. *Nature Rev. Mol. Cell Biol.* **2,** 107–117 (2001).
23. Ohya, T. *et al.* Reconstitution of Rab- and SNARE-dependent membrane fusion by synthetic endosomes. *Nature* **459,** 1091–1097 (2009).
24. Bucci, C. *et al.* Co-operative regulation of endocytosis by three Rab5 isoforms. *FEBS Lett.* **366,** 65–71 (1995).
25. Wucherpfennig, T., Wilsch-Brauninger, M. & Gonzalez-Gaitan, M. Role of *Drosophila* Rab5 during endosomal trafficking at the synapse and evoked neurotransmitter release. *J. Cell Biol.* **161,** 609–624 (2003).
26. Morrison, H. A. *et al.* Regulation of early endosomal entry by the *Drosophila* tumor suppressors Rabenosyn and Vps45. *Mol. Biol. Cell* **19,** 4167–4176 (2008).
27. Bucci, C. *et al.* The small GTPase rab5 functions as a regulatory factor in the early endocytic pathway. *Cell* **70,** 715–728 (1992).
28. Akinc, A. *et al.* Targeted delivery of RNAi therapeutics with endogenous and exogenous ligand-based mechanisms. *Mol. Ther.* **18,** 1357–1364 (2010).
29. Del Conte-Zerial, P. *et al.* Membrane identity and GTPase cascades regulated by toggle and cut-out switches. *Mol. Syst. Biol.* **4,** 206 (2008).
30. Heinrich, R. & Rapoport, T. A. Generation of nonidentical compartments in vesicular transport systems. *J. Cell Biol.* **168,** 271–280 (2005).
31. Serio, G. *et al.* Small GTPase Rab5 participates in chromosome congression and regulates localization of the centromere-associated protein CENP-F to kinetochores. *Proc. Natl Acad. Sci. USA* **108,** 17337–17342 (2011).
32. Akinc, A. *et al.* A combinatorial library of lipid-like materials for delivery of RNAi therapeutics. *Nature Biotechnol.* **26,** 561–569 (2008).
33. Love, K. T. *et al.* Lipid-like materials for low-dose, *in vivo* gene silencing. *Proc. Natl Acad. Sci. USA* **107,** 1864–1869 (2010).
34. Christoforidis, S., McBride, H. M., Burgoyne, R. D. & Zerial, M. The Rab5 effector EEA1 is a core component of endosome docking. *Nature* **397,** 621–625 (1999).
35. Collinet, C. *et al.* Systems survey of endocytosis by multiparametric image analysis. *Nature* **464,** 243–249 (2010).
36. Chen, P. I., Kong, C., Su, X. & Stahl, P. D. Rab5 isoforms differentially regulate the trafficking and degradation of epidermal growth factor receptors. *J. Biol. Chem.* **284,** 30328–30338 (2009).
37. Mukherjee, S., Ghosh, R. N. & Maxfield, F. R. Endocytosis. *Physiol. Rev.* **77,** 759–803 (1997).
38. Schroeder, B. M. M. in *The Liver: Biology and Pathobiology* 5th edn (eds Arias, I. *et al.*) Ch. 7 107–123 (Wiley-Blackwell, 2009).
39. Wolfsdorf, J. I. & Weinstein, D. A. Glycogen storage diseases. *Rev. Endocr. Metab. Disord.* **4,** 95–102 (2003).
40. van der Bliek, A. M. *et al.* Mutations in human dynamin block an intermediate stage in coated vesicle formation. *J. Cell Biol.* **122,** 553–563 (1993).
41. Shen, H. *et al.* Constitutive activated Cdc42-associated kinase (Ack) phosphorylation at arrested endocytic clathrin-coated pits of cells that lack dynamin. *Mol. Biol. Cell* **22,** 493–502 (2011).
42. Kipp, H., Pichetshote, N. & Arias, I. M. Transporters on demand: intrahepatic pools of canalicular ATP binding cassette transporters in rat liver. *J. Biol. Chem.* **276,** 7218–7224 (2001).
43. Wang, L. & Boyer, J. L. The maintenance and generation of membrane polarity in hepatocytes. *Hepatology* **39,** 892–899 (2004).
44. Wakabayashi, Y., Dutt, P., Lippincott-Schwartz, J. & Arias, I. M. Rab11a and myosin Vb are required for bile canalicular formation in WIF-B9 cells. *Proc. Natl Acad. Sci. USA* **102,** 15087–15092 (2005).
45. Lawe, D. C. *et al.* Sequential roles for phosphatidylinositol 3-phosphate and Rab5 in tethering and fusion of early endosomes via their interaction with EEA1. *J. Biol. Chem.* **277,** 8611–8617 (2002).
46. Renaud, G., Hamilton, R. L. & Havel, R. J. Hepatic metabolism of colloidal gold-low-density lipoprotein complexes in the rat: evidence for bulk excretion of lysosomal contents into bile. *Hepatology* **9,** 380–392 (1989).
47. Damke, H., Baba, T., van der Bliek, A. M. & Schmid, S. L. Clathrin-independent pinocytosis is induced in cells overexpressing a temperature-sensitive mutant of dynamin. *J. Cell Biol.* **131,** 69–80 (1995).
48. Koenig, J. H. & Ikeda, K. Transformational process of the endosomal compartment in nephrocytes of *Drosophila melanogaster*. *Cell Tissue Res.* **262,** 233–244 (1990).
49. Wakabayashi, Y., Lippincott-Schwartz, J. & Arias, I. M. Intracellular trafficking of bile salt export pump (ABCB11) in polarized hepatic cells: constitutive cycling between the canalicular membrane and rab11-positive endosomes. *Mol. Biol. Cell* **15,** 3485–3496 (2004).

Supplementary Information is linked to the online version of the paper at www.nature.com/nature.

Acknowledgements We acknowledge K. Simons, E. Knust, C. Fetzer, T. Galvez, G. O'Sullivan and M. P. McShane for discussions and comments on the manuscript. We thank W. John and A. Muench-Wuttke from the Biomedical Services Facility for mouse care and injections. We acknowledge J. Peychl for the management of the Light Microscopy Facility and K. Manygoats as well as J.-M. Verbavatz for their support. We thank B. Bettencourt and J. Hettinger for siRNA design and serum biochemistry assays, respectively. This work was financially supported by the Virtual Liver initiative (http://www.virtual-liver.de), funded by the German Federal Ministry of Research and Education (BMBF), the Max Planck Society (MPG) and the DFG. A.Z. was supported by a grant from Marie Curie Action, Intra-European Fellowship (fp7-people-ief-2008) and J.G. from an EMBO long-term fellowship.

Author Contributions M.Z. and V.K. conceived the project and M.Z. directed it. A.Z. designed and directed the animal injection experiments, and performed the stainings and imaging of liver sections. J.G. and A.Z. co-developed the staining procedures for the tissue sections. J.G.H. helped A.Z. to establish the hepatocyte isolation technique. A.Z. established the primary culture, developed the endocytosis assays, staining protocols and the knockdown technique with LNPs in primary hepatocytes. J.G. performed the electron microscopy analysis and quantifications, and the sectioning of liver tissue. R.L.B. selected siRNAs and validated their efficacy and specificity *in vitro* and *in vivo*, and designed, performed and analysed some *in vivo* experiments. H.E.-B. prepared the siRNAs into lipidoid-based formulations and analysed them. S.K. and C.G.P. performed the synthesis and analysis of siRNAs. V.M.R. designed, performed and analysed the 5′RACE assay. H.N. performed the RT–PCR in primary hepatocytes. S.S. under the supervision of A.Z. and J.G. performed the western blot analysis and performed the hepatocyte isolation and primary culturing under the supervision of A.Z.; G.M. under the supervision of Y.K. adapted the QMPIA for primary hepatocytes and liver tissue and performed the image analysis. Y.K. and P.dC.-Z. developed the mathematical model. M.Z., Y.K., A.Z. and J.G. wrote the manuscript, R.L.B. and V.K. participated in the editing.

Author Information Reprints and permissions information is available at www.nature.com/reprints. The authors declare no competing financial interests. Readers are welcome to comment on the online version of this article at www.nature.com/nature. Correspondence and requests for materials should be addressed to M.Z. (zerial@mpi-cbg.de).